Structural insights into styrylquinolines analogs as tubulin polymerization inhibitors: In silico Approach

Prerna Chourasia [1], **Vivek Asati** [2], **Shivangi Agarwal** [1], **Mitali Mishra** [1], **Varsha Kashaw** [3], **Ratnesh Das** [4], **and Sushil Kumar Kashaw** [1, *]

[1] Integrated Drug Discovery Research Laboratory, Department of Pharmaceutical Sciences, Dr.Harisingh Gour University (A Central University), Sagar (MP), India

[2] Department of Chemistry, ISF College of Pharmacy, Moga-Punjab

[3] Sagar Institute of Pharmaceutical Sciences, Sagar (M.P.)

[4] Department of Chemistry, Dr. Harisingh Gour University (A Central University), Sagar (MP), India

Abstract: Cancer is one of the fastest-growing epidemics that affect millions yearly. A handful of anticancer drugs are available on the market, but they produce undesirable side effects. Currently, tubulin inhibitors targeting the colchicine binding site are considered an important target due to their structural simplicity and favorable pharmacokinetics with fewer side effects. Different researchers conducted many studies to discover a novel tubulin inhibitor targeting the colchicine binding site with high safety and potency. In the present study, we performed computational analysis of 48 styrylquinolines analogs obtained from literature using different drug designing tools. The pharmacophore mapping study was conducted to identify the important pharmacophoric features essential for biological activity. Atom-based 3D-QSAR (3-dimensional quantitative structure-activity relationship) analysis was carried out to know the contribution of different atoms to model development. The generated model showed a statistically significant coefficient of determinations for the training and test sets. The best QSAR model was selected based on R^2 (0.8624) and Q^2 (0.6707) values. Contour plot analysis of the developed model unveiled the chemical features necessary for tubulin inhibition. A docking study was performed on potent styrylquinoline analog 9VII-f(46), which shows the highest SP docking scores (-5.494). ADME (Absorption, distribution, metabolism, and excretion) analysis provides valuable information about the drugability of newly designed compounds.

Keywords: Colchicine binding site; Styrylquinolines analogs; Pharmacophore mapping; Atom-based 3D-QSAR analysis; Docking study.

1. Introduction

Cancer is considered to be any of a large number of diseases characterized by the development of abnormal cells that divide uncontrollably and can migrate and destroy normal body tissue [1]. It is considered the second-leading cause of death [2] and was estimated to be responsible for ten million deaths globally in 2020 [3-5]. The prevalence & risk factor associated with it is an alarming concern globally [6]. A handful of different categories of anticancer drugs are available in the market, like Abitrexate (Methotrexate injection), Abraxane (Paclitaxel with albumin injection), and Adriamycin (Doxorubicin) [7]. Though cancer is not controllable in many cases, these agents cause undesirable side effects like anemia, appetite loss, bleeding and bruising (thrombocytopenia), hair loss, constipation, skin changes or reactions, etc. [8-10]. So, there is an utmost need to develop novel anticancer agents to minimize all those side effects and improve the quality of life. Microtubules are recognized as an excellent target for cancer chemotherapeutics which can cause apoptosis of cancer cells by disrupting microtubule dynamics [11-15]. Four unique binding sites in tubulin are present to which taxanes, vinca alkaloids, laulimalide, and colchicine bind, respectively [16-21]. Microtubule targeting agents that target the vinca site and taxanes (e.g., vincristine and paclitaxel, respectively) are highly potent and have been approved for clinical use [22-25]. However, their clinical usefulness is hampered for several reasons, such as developing multi-drug resistance (MDR), poor water solubility, and pharmacokinetics [26]. Tubulin inhibitors targeting the colchicine binding site can overcome the drawbacks due to their structural simplicity and favorable pharmacokinetics [14]. In contrast to agents binding to the other three sites, colchicine interacts with high affinity to tubulin and becomes copolymerized into microtubules [27-29]. Colchicine

binding to β-tubulin leads to curved tubulin dimer due to a steric clash between colchicine and α-tubulin, which inhibits microtubule assembly. [30-32]. The literature survey revealed that several analogs of tubulin inhibitors targeting the colchicine binding site have been synthesized, evaluated, and reported by researchers for the potential binding interactions with active site amino acid residues of tubulin. Several antitubulin agents targeting the colchicine binding site have been marketed as potential anticancer agents, such as colchicine (approved in 2009 by FDA), combretastatin (in phase I), and 2-Methoxyestradiol (in phase I), and some are under different phases of clinical trials. Recently, an FDA-approved drug, fosbretabulin (combretastatin A-4 phosphate), which is utilized for treating thyroid cancer, targets specifically the colchicine binding site. AVE8062 (ombrabulin, 5) is another CA-4 analog that exerts its anticancer effect by disrupting tumor blood vessel formation. It is also effective against several cancer cells that are resistant to taxanes. In a phase I study,

the combination of AVE8062 with docetaxel was well tolerated. A phase III study is currently ongoing for advanced cancer treatment. In the present study, we have attempted to perform computational analyses using drug-designing tools on 48 styrylquinolines derivatives reported in the literature [33]. The pharmacophore mapping was performed to establish the relationship between important pharmacophore features responsible for biological activity. Atom-based QSAR studies were conducted to investigate the contribution of each atom to the model. Molecular docking studies suggest key molecular interactions at the active site of the tubulin surrounded by amino acids. These studies (i.e., Pharmacophore mapping, Atom-based 3D-QSAR study, Molecular docking, and ADME property prediction) provided complementary information that may be useful in the future. The flow of work of computational analysis is given in Fig. 1.
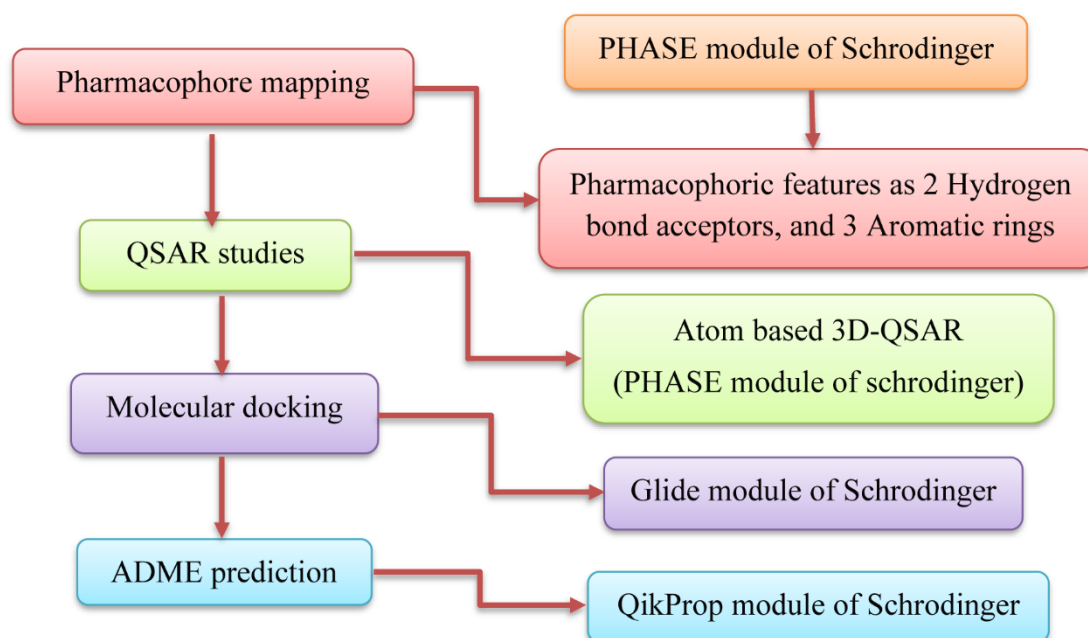

ss

Figure 1. Flow of work of computational analysis

2. Materials and methods

2.1. Selection of data

48 styrylquinoline analogs reported in the literature [33] were subjected to 3D-QSAR analysis, pharmacophore mapping, and molecular docking.

The dataset's structures were sketched using ChemDraw Ultra 12.0 software and saved in '.mol2' format. The common core of styrylquinoline analogs is presented as (1), and the substituted groups with biological activities are shown in Table 1.
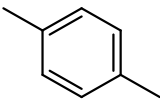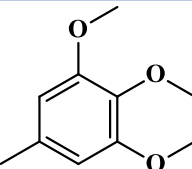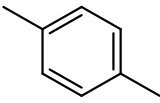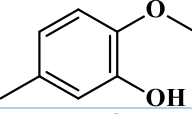

(1)
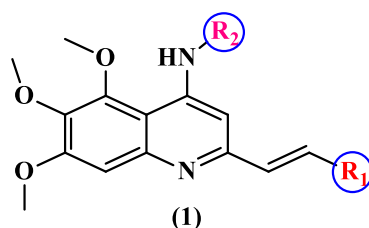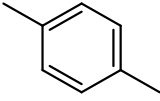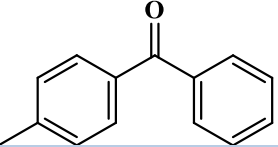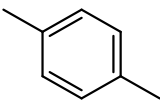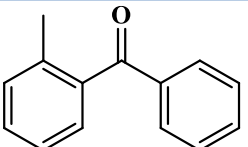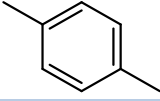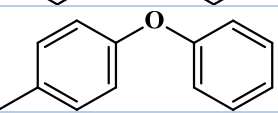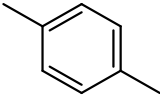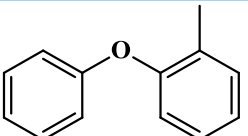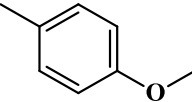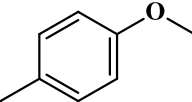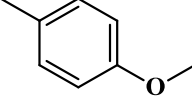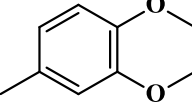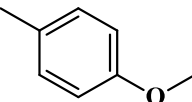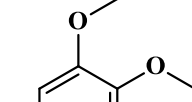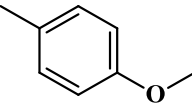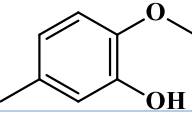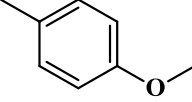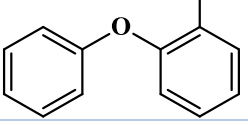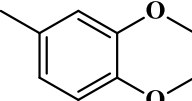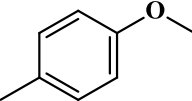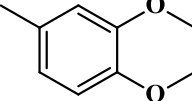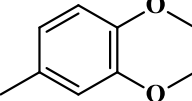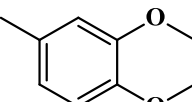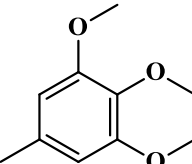
Atom-based 3D-QSAR studies were performed by Schrodinger MAESTRO' v12.1. Ligand was prepared using the LigPrep module of Maestro v12.1.
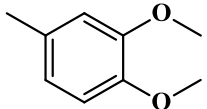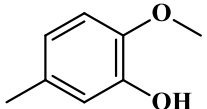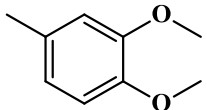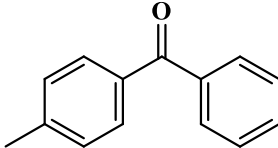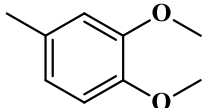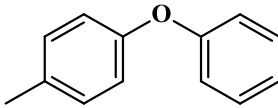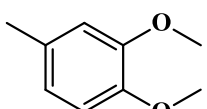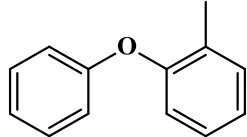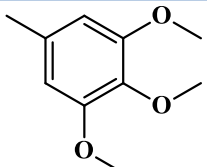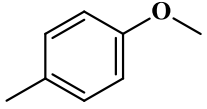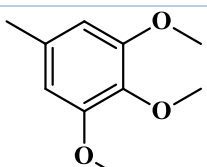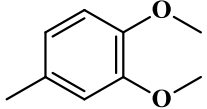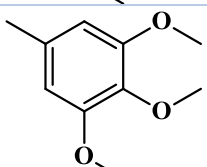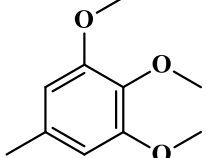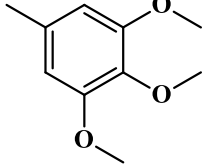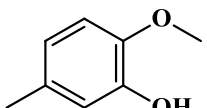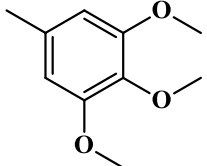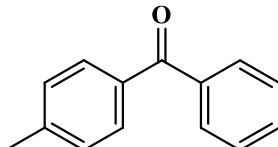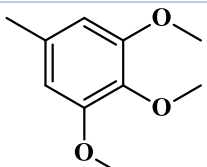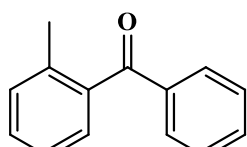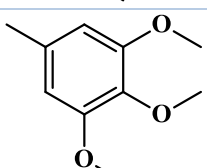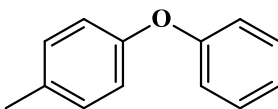
Pharmacophore mapping and docking analysis were done using the PHASE and Glide module of Schrodinger Maestro v12.1 software.
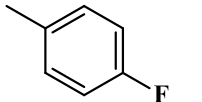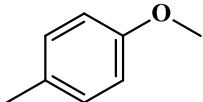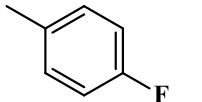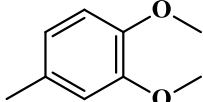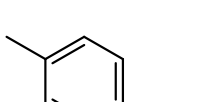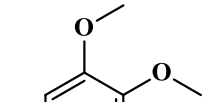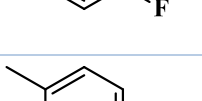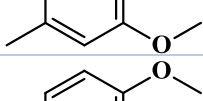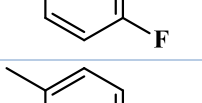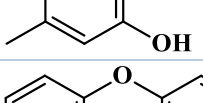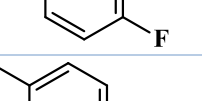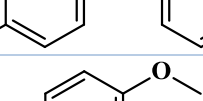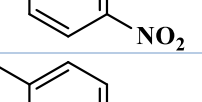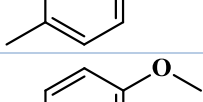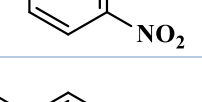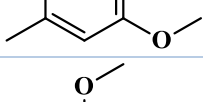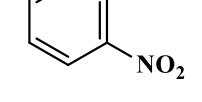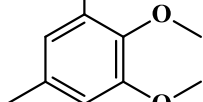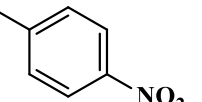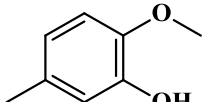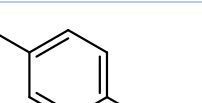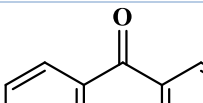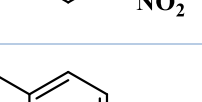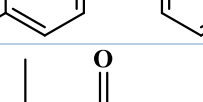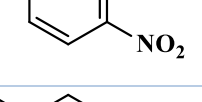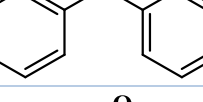
Table 1. Styrylquinoline analogs with their IC_{50} and pIC_{50} values.
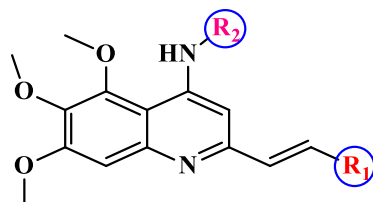
S.No.	Compounds	Structures		Activity (µm)	
		R₁	R₂	IC_{50} value	pIC_{50} value
1.	9I-a(1)			7.53	5.12
2.	9I-b(2)			5.57	5.25
3.	9I-c(3)			2.18	5.66
4.	9I-d(4)			3.31	5.48
5.	9I-e(5)			66.23	4.18
6.	9I-f(6)			10.18	4.99
7.	9I-g(7)			10.7	4.97
8.	9I-h(8)			9.17	5.04
9.	9II-a(9)			4.58	5.34
10.	9II-b(10)			3.06	5.51

11.	9II-c(11)			1.32	5.88
12.	9II-d(12)			2.32	5.63
13.	9II-e(13)			29.73	4.53
14.	9II-f(14)			10.92	4.96
15.	9II-g(15)			7.23	5.14
16.	9II-h(16)			11.96	4.92
17.	9III-a(17)			4.36	5.36
18.	9III-b(18)			3.46	5.46
19.	9III-c(19)			2.2	5.66
20.	9III-d(20)			3.44	5.46
21.	9III-h(21)			8.77	5.06
22.	9IV-a(22)			3.03	5.52
23.	9IV-b(23)			1.7	5.77
24.	9IV-c(24)			0.5	6.30

25.	9IV-d(25)			2.28	5.64
26.	9IV-e(26)			13.02	4.89
27.	9IV-g(27)			4.03	5.39
28.	9IV-h(28)			7.09	5.15
29.	9V-a(29)			3.95	5.40
30.	9V-b(30)			2.88	5.54
31.	9V-c(31)			1.49	5.83
32.	9V-d(32)			1.95	5.71
33.	9V-e(33)			14.28	4.85
34.	9V-f(34)			25.43	4.59
35.	9V-g(35)			4.12	5.39

36.	9VI-a(36)			3.21	5.49
37.	9VI-b(37)			1.27	5.90
38.	9VI-c(38)			1.08	5.97
39.	9VI-d(39)			1.17	5.93
40.	9VI-g(40)			11.73	4.93
41.	9VII-a(41)			3.17	5.50
42.	9VII-b(42)			1.44	5.84
43.	9VII-c(43)			0.38	6.42
44.	9VII-d(44)			7.41	5.13
45.	9VII-e(45)			9.14	5.04
46.	9VII-f(46)			9.64	5.02
47.	9VII-g(47)			3.77	5.42
48.	9VII-h(48)			18.43	4.73

2.2. 3D-QSAR analysis

For 3D-QSAR, the compounds were divided into training and test set. The training set covers 70% of total molecules, whereas the remaining 30% of compounds are taken as a test set. For the best 3D QSAR model generation, the molecules were aligned

to find the best alignment and standard features (Fig. 2). This alignment is based on the maximum standard core structure of molecules using the most active molecule in the dataset template. A statistically significant atom-based 3D-QSAR model was developed via partial least-squares (PLS) regression, where an increase in statistical significance and predictivity was observed up to five PLS factors [34-37]. The various statistical parameters of the 3D-QSAR model are used to evaluate the robustness of the QSAR model. A scatter plot was constructed between actual and predicted activity to confirm minimal diversity in the biological activities between training and test set molecules, respectively [38-40].
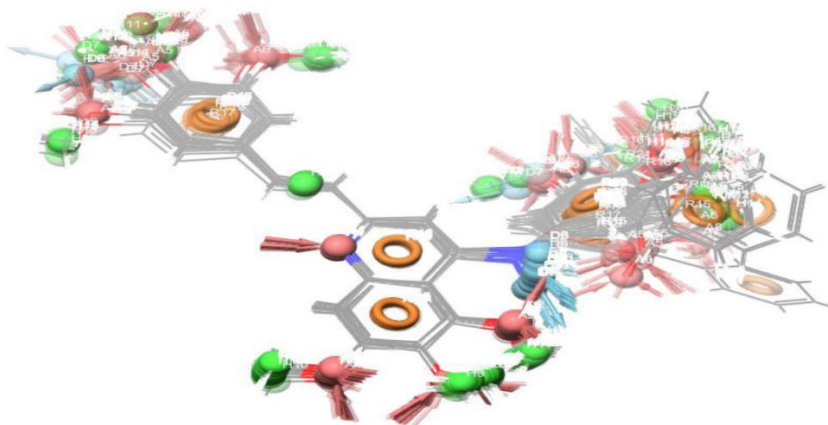
Figure 2. Molecular alignment of all the compounds in the datasets for tubulin inhibitors

2.3. Pharmacophore mapping

We identified the critical pharmacophoric features by pharmacophore mapping using the PHASE module to set up the relationship between molecular descriptors and biological activity. The compounds from the dataset were subjected to the LigPrep module to produce high-quality 3D structures of all atoms with correct chirality [41]. In the present study, the module provides 2 standard chemical features, i.e., ring aromaticity (R) & hydrophobic group (H) (Fig. 3(A)).
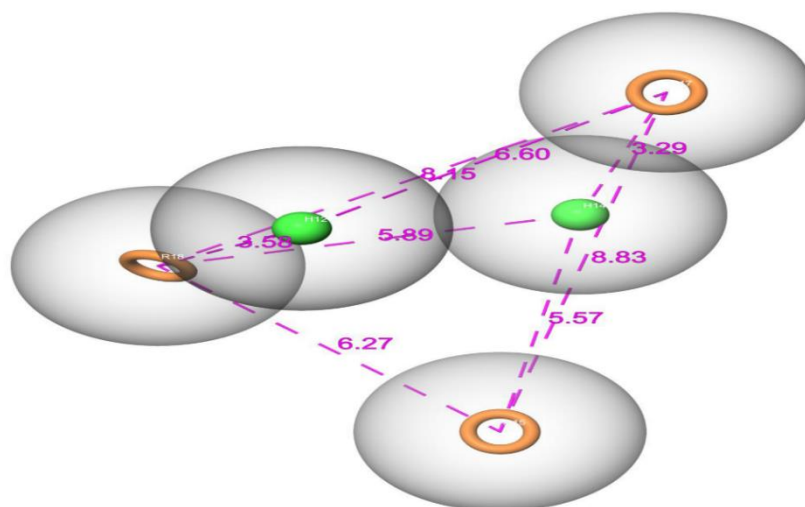
Figure 3(A). Common pharmacophoric features of the generated module

To find the exact positions of these features, we have used a distance calculation tool inbuilt into the module to ascertain the inter-features distance map shown in Fig. 3(B). The PHASE module generated various pharmacophore hypotheses and computed their survival scores. Among those, the best was selected, containing the essential features responsible for activity [42,43].
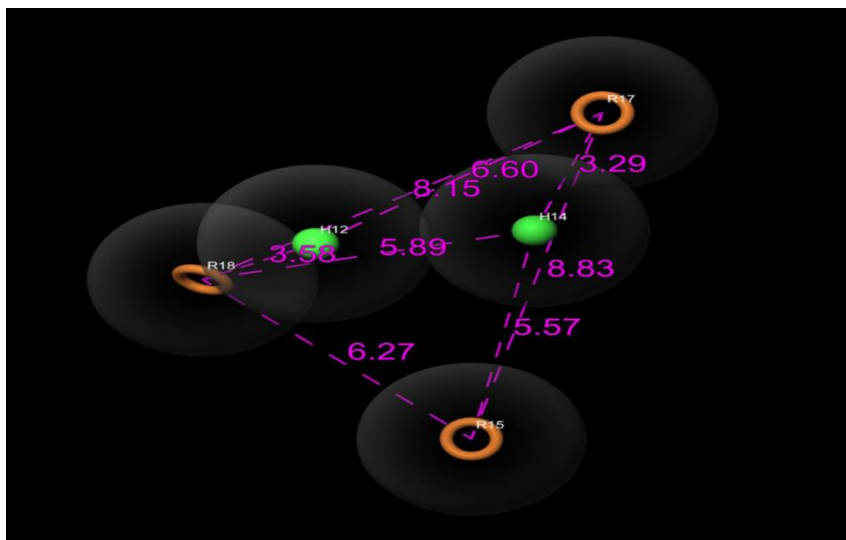
Figure 3(B). Inter-featuric distance map of HHRRR_1 hypothesis

2.4. Pharmacophore hypothesis generation

The pharmacophore hypotheses were created based on the standard pharmacophoric features of all 48 compounds. A maximum of five pharmacophoric sites were selected to develop a common pharmacophore hypothesis. Further, five-point pharmacophore hypotheses matching all active ligands were generated with a box size of 1 Å, and minimum inter-site distances between two features were set at 2 Å. Among the generated hypothesis, the best was selected based on the Phase hypothesis score, site score, survival score, Selectivity score, volume score, vector score, number of matches, and energy terms [44,45].

2.5. Molecular Docking

To determine the binding interaction of compounds containing essential pharmacophoric features, molecular docking studies were performed through the Glide module of Schrodinger Maestro v12.1 [46] on styrylquinoline analogs to the binding site of tubulin. The 3D-crystal structure of the protein was obtained from the protein data bank and processed through the protein preparation wizard in Maestro Wizard v12.1. Water molecules were removed, and hydrogen atoms and charges were automatically added to the protein molecules by refinement step using the default force field OPLS_ 3e. After optimization, binding pockets in the receptor were located, and the docking results were obtained with different docked ligand conformations [47-51].

2.6. ADME property predictions

The drug-like activity of the ligand molecule was identified using ADME properties by the QikProp module of Schrodinger [52]. This module is a quick, accurate, and easy-to-use ADME prediction program designed to produce certain descriptors related to ADME. It predicts physicochemical descriptors and pharmacokinetic properties in terms of #star: it defines the number of property or descriptor values that fall outside the 95% range of similar values for known drugs. A large number of stars suggests that a molecule is less drug-like than molecules with few stars. The following properties and descriptors are included in the determination of #stars: MW, dipole, IP, EA, SASA, FOSA, FISA, PISA, WPSA, PSA, volume, #rotor, donorHB, accptHB, glob, QPpolrz, QPlogPC16, QPlogPoct, QPlogPw, QPlogPo/w, logS, QPLogKhsa, QPlogBB, #metabol. The range of recommended values for #star is 0-5. ADME properties determine the drug-like activity of ligand molecules based on Lipinski's rule of five. The rules are: mol_MW < 500, QPlogPo/w < 5, donorHB ≤ 5, accptHB ≤ 10. Compounds that satisfy these rules are considered drug-like. Jorgensen's rules of three are QPlogS > -5.7, QP PCaco > 22 nm/s, # Primary Metabolites < 7 [53].

3. Results and discussion

3.1. Pharmacophore modeling

We generated pharmacophore hypotheses of all the selected compounds from the dataset to identify standard features essential for biological activity. The generated hypotheses comprise five pharmacophoric features, i.e., 2 hydrophobic interactions (H12, H14), 3 aromatic rings (R15, R17, R18). These features display a crucial role in the inhibitory potencies of compounds toward the target. The field distances between H12-H17, H12-R18, H14-R15, H14-R17, H14-R18, R15-R17, R15-R18, and R17-R18 were found to be 6.60 Å, 3.58 Å, 5.57Å, 3.29 Å, 5.89 Å, 8.83 Å, 6.27 Å and 8.15Å respectively. HHRRR_1 was selected as the best hypothesis among the generated ideas based on the scoring values of different parameters.

The generated pharmacophore model can be evaluated by two tools, namely % Screen plot & ROC plot. The percent screen plot is the curve between the percentage of actives recovered And the percentage of ligands screened for the hypothesis. The ROC plot is drawn between sensitivity and specificity. The ROC

curve that passes through the upper left corner shows 100% sensitivity and 100% specificity. Therefore, this suggests that the method's accuracy depends on the closeness of the curves in the upper left corner. The present study showed that both the percent screen

plot and ROC plot are in the extreme left corner, as shown in Fig. 4(A) and   Fig.4 (B), which suggests the accuracy of the hypotheses generated by the PHASE module.

(A)

(B)
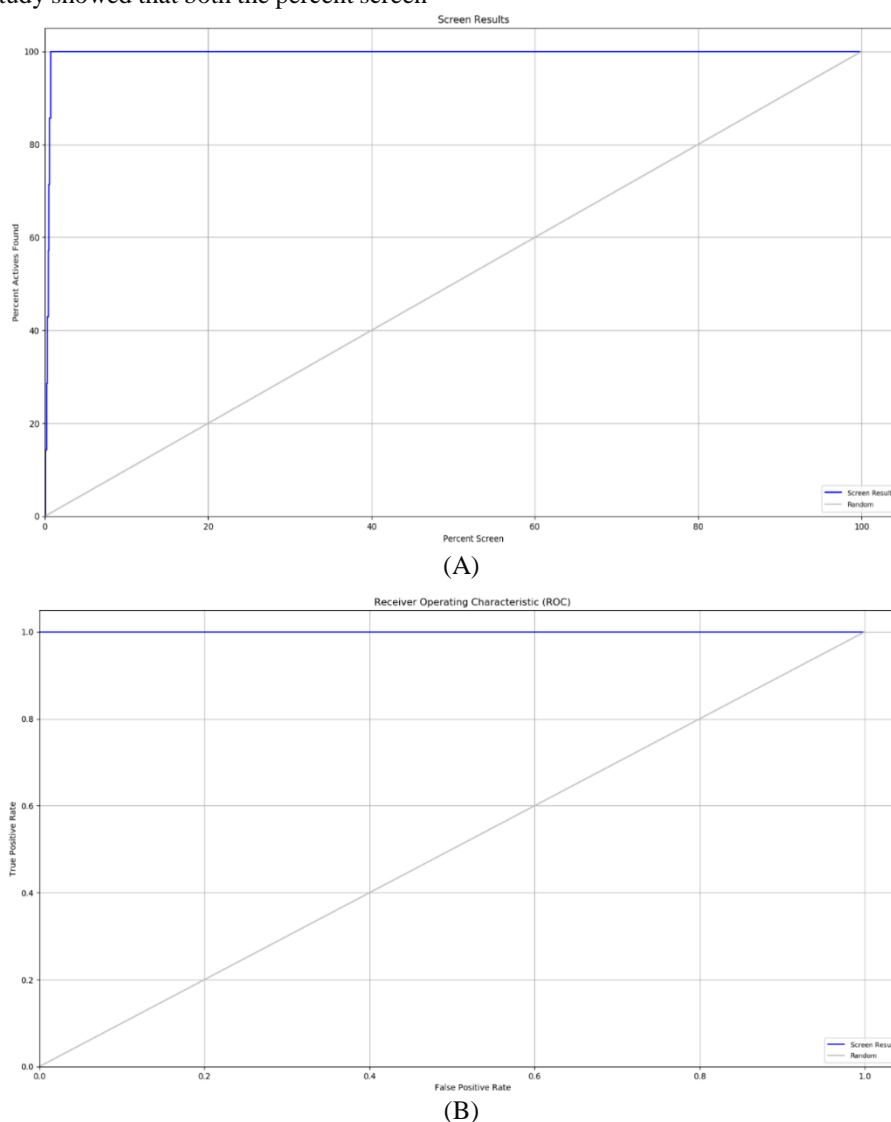
Figure 4. (**A**) percent screen plot; (**B**) ROC plot

3.2. Atom-based 3D-QSAR analysis

The QSAR results obtained through the Maestro v12.1 module show the statistically significant coefficient for the training and test sets. Each row of the QSAR statics table was developed via partial least-squares (PLS) regression, where molecules were clustered by a PLS factor of 5. Several statistical parameters such as SD, R^2, F, P, RMSE (Root mean square error), Q^2, and Pearson-R were selected to evaluate the robustness of the QSAR model. For good predictivity and robust significance, the QSAR model should have a significant value of R^2 (correlation for training set molecules), Q^2 (cross-validated correlation for test set molecules), Pearson-R, and F-value. The R^2 value should be preferably greater than 0.6, and Q^2 and Pearson-R should be greater than 0.5.

The RMSE should be low, along with a small value of the variance ratio, p. All five models generated by the module are shown in   Table 3. Based on the above knowledge, we have chosen 5th model as a significant QSAR model due to higher Q^2 and R^2 values of 0.6707 and 0.8624, respectively. Atom type fraction segment displayed the fraction contributed by each atom type for each number of PLS factors used in the QSAR model, as summarized in Table 4.

The correlation between experimental activity and predicted activity of training and test set in the form of scatter plots are shown in Fig. 5. This scattered plot shows the uniform distribution of training set molecules throughout the straight line passing through the origin (0, 0).

Table 2. Desired values for the statistically significant model.

Validation Parameters	Desired value
Squared cross-validation coefficient (q^2)	>0.5
Squared non-cross-validation coefficient(r^2)	>0.5
Standard error of estimate (SEE)	Smaller is better (<0.3)
Predictive factorr^2 (r^2_{pred})	>0.5

Table 3. Atom-based 3D-QSAR statistics table.

# Factors	SD	R^2	R^2CV	F	P	RMSE	Q^2	Pearson-r
1	0.2384	0.7412	0.6218	106	2.07E-12	0.21	0.5612	0.8128
2	0.2148	0.7955	0.6356	70	3.92E-13	0.18	0.6655	0.8533
3	0.1982	0.8308	0.5922	57.3	1.39E-13	0.2	0.5866	0.8041
4	0.1884	0.8514	0.5413	48.7	1.30E-13	0.18	0.6704	0.8423
5	0.1841	0.8624	0.4783	41.4	2.81E-13	0.18	0.6707	0.8475

Table 4. Atom type fraction.

# Factors	H-bond donor	Hydrophobic/non-polar	Negative ionic	Electron-withdrawing
1	0.036	0.683	0.014	0.267
2	0.031	0.707	0.017	0.245
3	0.033	0.722	0.024	0.221
4	0.035	0.717	0.029	0.219
5	0.038	0.72	0.028	0.214

(A)
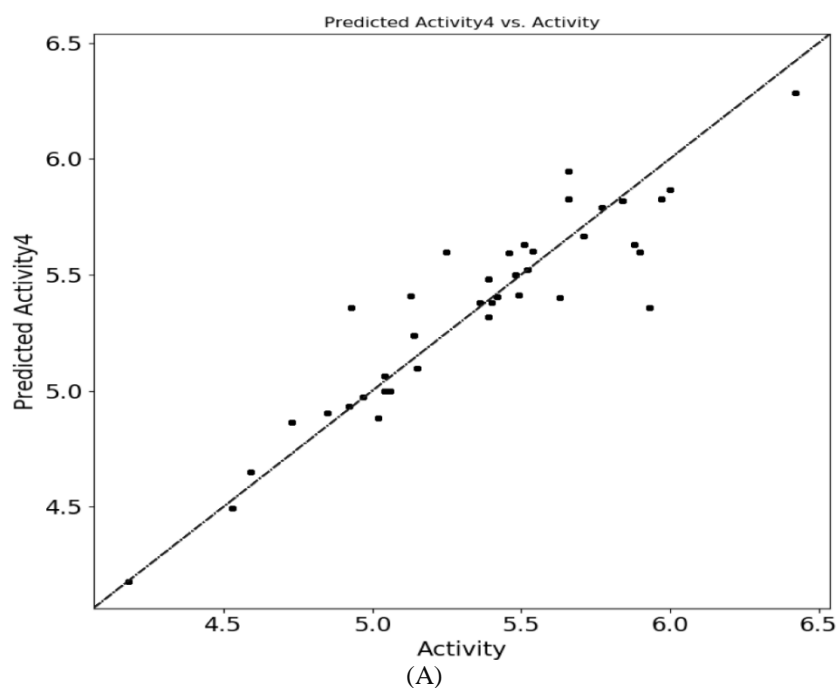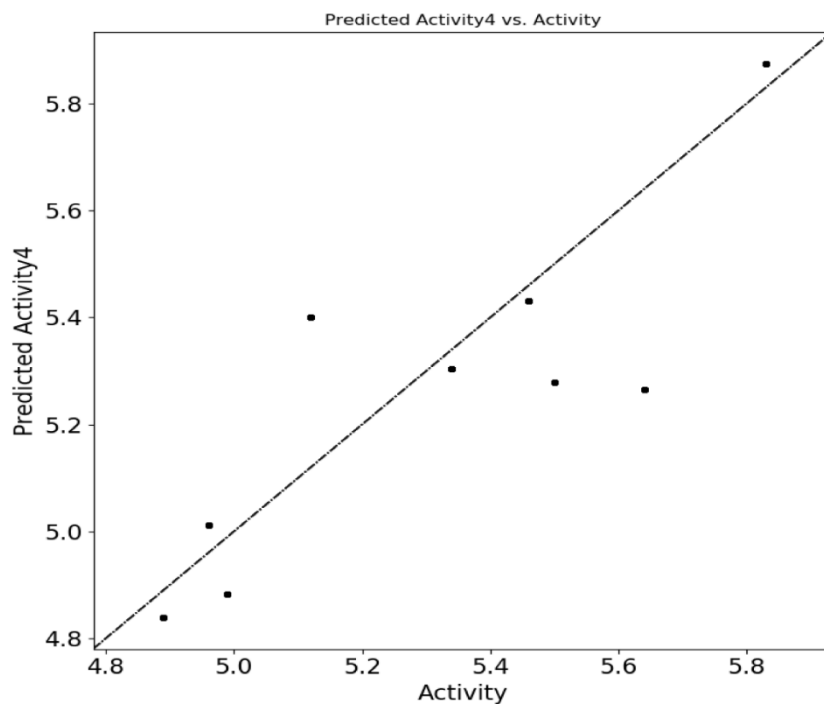
(B)

Figure 5. Scattered plot of experimental activity Vs predicted activity (A) training set; (B) test set molecules

3.3. QSAR Contour plot analysis

The result obtained by 3D-QSAR were analyzed using contour maps to understand the effect of substituents at different positions on the potency and selectivity of inhibitors. The blue cubes indicate the regions of favorable interactions, whereas the red cubes indicate the regions of unfavorable interactions. The 3D-QSAR model was applied to the most active compound to obtain significant favorable and unfavorable regions for hydrogen bond donor, hydrophobic, and electron-withdrawing groups.

For the hydrophobic character in the most active compound (9I-f(6)), the appearance of blue cubes near the ortho position of the phenyl ring of stryrlquinoline moiety (Fig. 6(A)) shows that this position is favorable for hydrophobic substitution. On

the other hand, the presence of red cubes around the benzophenone moiety and ethylene bridge indicates that these positions are unfavorable for hydrophobic substitution.

The hydrogen bond donating attributes is another important component impacting the activity. For example, in compound (9I-f(6)), the appearance of red cubes around NH group (Fig. 6(B)) indicates that this region is unfavorable for hydrogen bond donating groups.

The presence of red cubes around the oxygen atom of benzophenone moiety and near the NH bridge between styrylquinoline and benzophenone moiety (Fig. 6(C)) indicated the non-preference of electron-withdrawing groups at these positions.

(A)

(B)

(C)
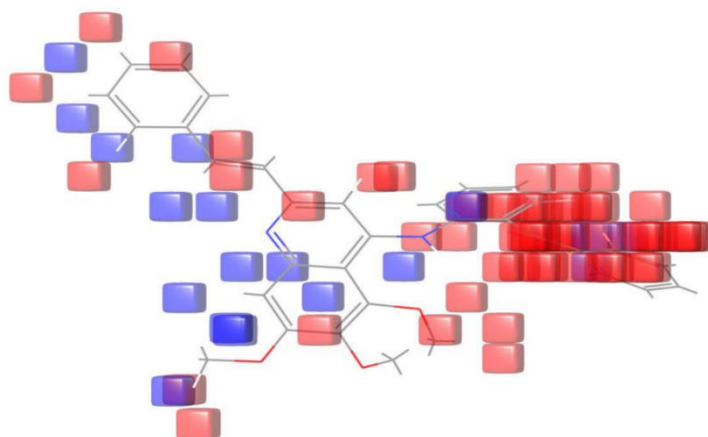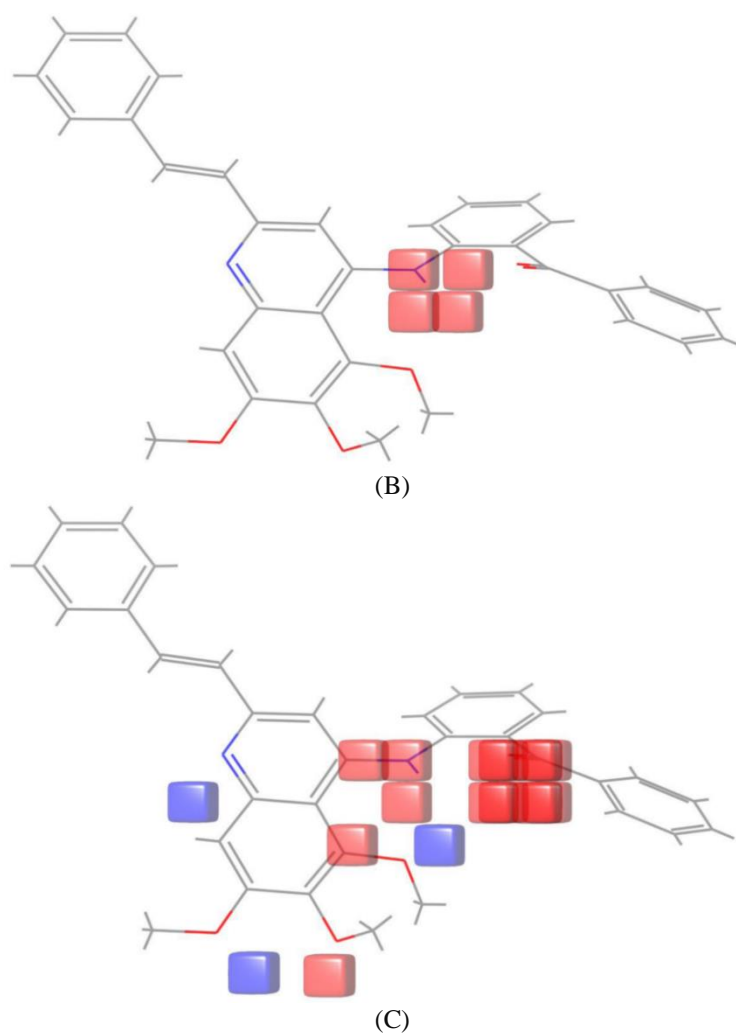
Figure 6. QSAR Contour plot to show the effect of substituents at different positions. The presence of blue cubes indicates the region of favorable interaction. In contrast, the appearance of red cubes indicates the unfavorable region for (A) Hydrophobic groups, (B) Hydrogen bond donors, and (C) Electron withdrawing groups.

(A)

(B)

Figure 7. Diagram of compound 9VII-f(46) interacting with tubulin: (A) 2D, (B) 3D

3.4. Molecular docking analysis

The potential interactions between the most potent derivatives and protein were performed using the Glide module of Schrodinger. All the styrylquinoline analogs were docked to the binding cavity of tubulin. The potent styrylquinoline analogs 9VII-f(46), 9VII-d(44), 9VII-c(43), 9VII-b(42) & 9IV-h(28), show the highest SP docking scores, i.e., -5.494, -5.494, -5.001, -4.611 and -4.336, respectively when interacted with TYR222, MG502, ARG276, GLN11, ASN204. The hydrogen bond and pi-pi stacking interactions were shown by purple & green colored arrows, respectively. Compound 9VII-f(46) shows 1 hydrogen bond with TYR222 at the oxygen atom of benzophenone moiety and 1 pi-pi stacking interaction with TYR222 at the benzene ring of styrylquinoline moiety as shown in Fig. 7. Compound 9VII-d(44), 9VII-c(43) and 9VII-b(42) form 1 hydrogen bong with ARG276 amino acid at ether group of quinoline moiety & 1 pi-pi stacking interaction as shown in Fig. 8. Compound 9IV-h(28) creates 3 hydrogen bonds, 2 with ASN204 at ether groups of benzene ring & 1 with the oxygen atom of benzophenone moiety. It also shows 1 pi-pi stacking interaction with TYR222 at the benzene ring, as shown in Fig. 9.

(A)

(B)

(C)

Figure 8. 2D Diagram of compounds interacting with tubulin: (A) 9VII-d(44), (B) 9VII-c(43) and (C) 9VII-b(42)
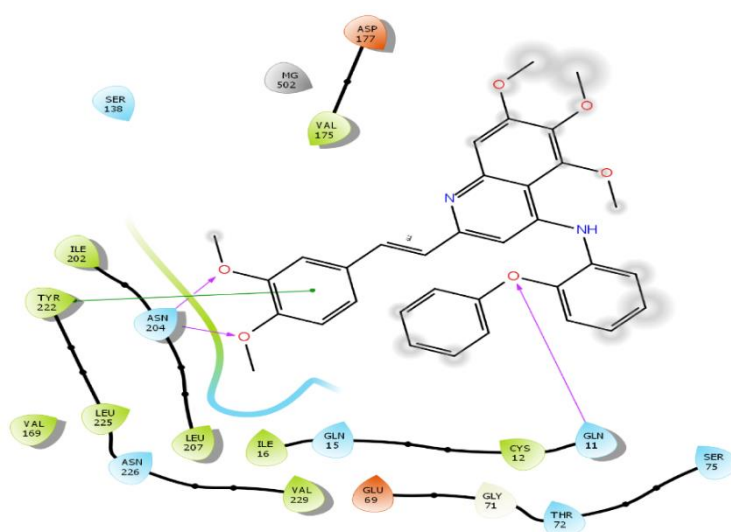
Figure 9. 2D Diagram of compound 9IV-h(28) interacting with tubulin

3.5. ADME prediction

The dataset's ADME properties of 48 styrylquinoline analogs were evaluated with the QikProp module of Schrodinger, as shown in Table 5. All compounds showed significant ADME properties like a molecular weight between 130.0 – 725.0, many hydrogen bond

acceptors between 2.0 – 20.0, several hydrogen bond donors between 0.0 – 6.0, number of rotatable bonds 0-15. None of the compounds shows CNS activity (– 2 (inactive), +2 (active)). All the predicted properties of styrylquinoline analogs satisfy Lipinski's rule of five and f Jorgensen's three.

Table 5. Result of ADME studies.

Molecules	#stars	#rotor	CNS	mol_MW	dipole	Donor HB	Acceptor HB	Rule Of Five	Rule Of Three
9l-a(1)	2	9	0	442.513	2.619	1	4.5	1	1
9I-b(2)	2	10	0	472.54	1.241	1	5.25	1	1
9l-c(3)	2	11	0	502.566	1.535	1	6	2	2
9I-d(4)	1	10	-1	458.513	1.353	2	5.25	1	1
9I-e(5)	5	10	0	516.595	3.865	1	5.75	2	1
9I-f(6)	4	10	0	516.595	4.164	0	4.75	2	1
9I-g(7)	4	10	0	504.584	1.631	1	4.25	2	1
9I-h(8)	5	10	0	504.584	2.066	1	4.25	2	1
9II-a(9)	3	9	0	456.54	1.278	1	4.5	1	2
9II-b(10)	2	10	0	486.566	1.374	1	5.25	1	2
9II-c(11)	2	10	0	486.566	1.374	1	5.25	1	2
9II-d(12)	4	10	-1	472.54	3.931	2	5.25	1	2
9II-e(13)	6	10	-1	530.622	3.418	1	5.75	2	1
9II-f(14)	6	10	0	530.622	4.089	0	4.75	2	1
9II-g(15)	6	10	0	518.611	2.235	1	4.25	2	1
9II-h(16)	6	10	0	518.611	2.111	1	4.25	2	1
9III-a(17)	2	10	0	472.54	1.576	1	5.25	1	2
9III-b(18)	3	11	0	502.566	1.583	1	6	2	2
9III-c(19)	2	12	0	532.592	4.23	1	6.75	2	2
9III-d(20)	1	11	-1	488.539	3.567	2	6	1	2
9III-h(21)	6	11	0	534.61	1.186	1	5	2	2
9IV-a(22)	2	11	0	502.566	3.311	1	6	2	2
9IV-b(23)	3	12	0	532.592	2.026	1	6.75	2	2
9IV-c(24)	3	13	0	562.618	4.084	1	7.5	2	2
9IV-d(25)	3	12	-1	518.565	4.306	2	6.75	2	2
9IV-e(26)	5	12	-1	576.648	4.721	1	7.25	2	1
9IV-g(27)	6	12	0	564.637	3.784	1	5.75	2	1
9IV-h(28)	6	12	0	564.637	2.876	1	5.75	2	2
9V-a(29)	3	12	0	532.592	3.311	1	6.75	2	2
9V-b(30)	3	13	0	562.618	4.97	1	7.5	2	2
9V-c(31)	5	14	-1	592.644	5.712	1	8.25	3	2

9V-d(32)	3	13	-1	548.591	5.36	2	7.5	2	2
9V-e(33)	4	13	-1	606.674	4.539	1	8	2	2
9V-f(34)	6	13	0	606.674	5.307	0	7	2	2
9V-g(35)	7	13	0	594.663	5.94	1	6.5	2	2
9VI-a(36)	2	9	1	460.504	4.583	1	4.5	1	1
9VI-b(37)	2	10	0	490.53	3.288	1	5.25	1	1
9VI-c(38)	2	11	0	520.556	3.679	1	6	2	2
9VI-d(39)	1	10	0	476.503	4.293	2	5.25	1	1
9VI-g(40)	1	10	0	476.503	4.293	2	5.25	1	1
9VII-a(41)	1	12	-2	489.527	3.294	3	5.5	1	1
9VII-b(42)	1	13	-2	519.553	2.723	3	6.25	2	2
9VII-c(43)	3	14	-2	549.579	4.085	3	7	3	2
9VII-d(44)	1	13	-2	505.526	4.552	4	6.25	1	2
9VII-e(45)	4	13	-2	563.609	4.274	3	6.75	2	1
9VII-f(46)	5	13	-2	563.609	4.853	2	5.75	2	1
9VII-g(47)	5	13	-2	551.598	4.158	3	5.25	2	1
9VII-h(48)	5	13	-2	551.598	2.991	3	5.25	2	1

4. Conclusion

In the present study, we used a computational approach to ascertain the best possible molecules from a dataset of 48 styrylquinoline analogs obtained from the literature. 3D pharmacophore model has been developed using the PHASE module of Schrodinger, and the best hypothesis, HHRRR_1, was selected. Atom-based 3D QSAR module generated through Maestro v12.1 module and the selected model showed a high coefficient of determination ($R^2 = 0.8624$) and cross-validation coefficient ($Q^2 = 0.6707$) with low RMSE (0.18) and SD (0.1841). The contour map analysis unveiled the importance of various features (hydrogen bond donor, hydrophobic group, electron-withdrawing groups) in determining the structural requirements necessary for binding the inhibitors. A molecular docking study was performed using the Glide module of Schrodinger into the binding site of tubulin. The receptor-ligand complex was stabilized by hydrogen bonding and pi-pi stacking interaction, and compound 9VII-f(46) shows the best docking score. The ADME analysis was performed through the QikProp module of Schrodinger, which provides an idea about the drug-like property and possible toxicity associated with the receptor. All the predicted properties of styrylquinoline analogs satisfy Lipinski's rule of five, which indicates their drug-like potential. I hope the present studies may be helpful to the researchers in the discovery of novel anticancer agents.

Conflict of interest

Authors do not have any conflict of interest

References

1. G.M. Cooper, The Cell: A Molecular Approach, 2nd edition. **2000**.
2. N.G. Zaorsky, T.M. Churilla, B.L. Egleston, S.G. Fisher, J.A. Ridge, E.M. Horwitz, J.E. Meyer, Causes of death among cancer patients, Annals of Oncology, **2017**, 28, 400-407.
3. A. Jemal, F. Bray, J. Ferlay, E. Ward, Global cancer statics, A cancer journal for clinicians, **2011**, 61(2), 69-90.
4. H. Sung, J. Ferlay, R.L. Siegel, M.Laversanne, I. Soerjomataram, A. Jemal, F. Bray, Global Cancer Statistics 2020: GLOBOCAN Estimates of incidence and Mortality Worldwide for 36 Cancers in 185 Countries, A Cancer Journal for Clinicians, **2021**, 71(3), 209-249.

5. M.E.A. de Kraker, A.J. Stewardson, S. Harbarth, Will 10 Million People Die a Year due to Antimicrobial Resistance by 2050?, Plos Medicine, **2016**, 13(11), e1002184.

6. H. Khil, S.M. Kim, S.E. Hong, H.M. Gil, E. Cheon, D.H. Lee, Y.A. Kim, N. Keum, Time trends of colorectal cancer incidence and associated lifestyle factors in South Korea, Scientific Reports, **2021**, 11, 2413.

7. S. Shrestha, R.S. Poudel, K.C. Bhuvan, B.K. Poudel, B. Sapkota, S. Sharma, A. Khadka, Price variation among different brands of anticancer medicines available in hospital pharmacies of Nepal, Journal of Pharmaceutical Policy and Practice, **2020**.

8. I. Ojima, X. Wang, Y. Jing, C. Wang, Quest for Efficacious Next-Generation Taxoid Anticancer Agents and Their Tumor-Targeted Delivery, Journal of natural products, **2018**, 81(3), 703-721.

9. A. Zarbo, A. Axelson, Common Cutaneous Side Effects of Anticancer Agents, Practical guide to dermatology, **2019**, 289-306.

10. A.F. Hood, Cutaneous side effects of cancer chemotherapy, The Medical clinics of North America, **1986**, 70(1), 187-209.

11. D. Sunil, P. Kamath, Indole-based tubulin polymerization inhibitors: An update on recent developments, Mini reviews in medicinal chemistry, **2016**, 16(18), 1470-1499.

12. K.S. Chan, C.G. Koh, H.Y. Li, Mitosis-targeted anticancer therapies: where they stand, Cell Death & Disease, **2012**.

13. J. Dinic, C. Rios-Luci, I. Karpaviciene, I. Cikotiene, M.P. Fernandes, J.M. Padron, CKTo353, a novel microtubule targeting agent, overcomes paclitaxel-induced resistance in cancer cells, Investigational New Drugs, **2020**, 584-598.

14. L. Li, D. Quan, J. Chen, J. Ding, J. Zhao, L. Lv, J. Chen, Design, synthesis, and biological evaluation of 1- substituted-2-aryl imidazoles targeting tubulin polymerization as potential anticancer agents, European Journal of Medicinal Chemistry, **2019**, 184, 111732.

15. A.L. Parker, M. Kavallaris, J.A. McCarroll, Microtubules and their role in cellular stress in cancer, Frontiers in Oncology, **2014**, 4, 153.

16. M.A. Jordan, L. Wilson, Microtubules as a target for anticancer drugs, Nature Reviews Cancer, **2004**, 4, 253-265.

17. L. Li, S. Jiang, X. Li, Y. Liu, J. Su, J. Chen, Recent advances in tri methoxyphenyl (TMP) based tubulin inhibitors targeting the colchicine binding site, European Journal of Medicinal chemistry, **2018**, 151, 482-494.

18. W. Liu, G. Wang, Z. Peng, Y. Li, Design, Synthesis and Biological Evaluation of Novel 4-(4-Methoxynaphthalen-1-yl)-5-arylpyrimidin-2-amines as Tubulin Polymerization Inhibitors,

19. Y. Wan, Y. Li, C. Yan, M. Yan, Z. Tang, Indole: A privileged scaffold for the design of anticancer agents, European Journal of Medicinal Chemistry, **2019**, 183, 111691.

20. H. Guo, X. Li, Y. Guo, L. Zhen, An overview of tubulin modulators deposited in protein data bank, Medicinal Chemistry Research, **2019**, 28, 927-937.

21. Y. Wang, H. Zhang, B. Gigant, Y. Yu, Y. Wu, X. Chen, Q. Lai, Z. Yang, Q. Chen, J. Yang, Structures of a diverse set of colchicine binding site inhibitors in complex with tubulin provide a rationale for drug discovery, The FEBS journal, **2015**, 283(1), 102-111.

22. E. Mukhtar, V.M. Adhami, H. Mukhtar, Targeting Microtubules by Natural Agents for Cancer Therapy, Molecular Cancer Therapeutics, **2014**.

23. A.F. Serpico, R. Visconti, D. Grieco, Exploiting immune-dependent effects of microtubule-targeting agents to improve efficacy and tolerability of cancer treatment, Cell Death & Disease, **2020**.

24. K.E. Arnst, Y. Wang, D.J. Hwang, Y. Xue, T. Costello, D. Hamilton, Q. Chen, J. Yang, F. Park, J.T. Dalton, D.D. Mliier, W. Li, A Potent, Metabolically Stable Tubulin Inhibitor Targets the Colchicine Binding Site and Overcomes Taxane Resistance, Cancer Research, **2018**.

25. V. Cermak, V. Dostal, M. Jelinek, L. Libusova, J. Kovar, D. Rosel, J. Brabek, Microtubule-targeting agents and their impact on cancer treatment, European Journal of Cell Biology, **2020**, 99(4), m151075.

26. S. Marchal, A.E. Hor, M. Millard, V. Gillon, L. Bezdetnaya, Anticancer Drug Delivery: An Update on Clinically Applied Nanotherapeutics, Drugs, **2015**, 75, 1601-1611.

27. S.B. Hastie, Interactions of colchicine with tubulin, Pharmacology & therapeutics, **1991**, 51(3), 377-401.

28. Y. Lu, J. Chen, M. Xiao, W. Li, D.D. Miller, An Overview of Tubulin Inhibitors That Interact with the Colchicine Binding Site, Pharmaceutical Research, **2012**, 29, 2943-2971.

29. E.C McLoughlin., N.M O'Boyle., "Colchicine-Binding Site Inhibitors from Chemistry to Clinic: A Review", Pharmaceuticals, 2020, 13(1):8.

30. R.A. Stanton, K.M. Gernert, J.H. Nettles, R. Aneja, Drugs that target dynamic microtubules: A new molecular perspective, Medicinal Research Reviews, **2011**, 31(3), 443-481.

31. X. Lv, C. He, C. Huang, G. Hua, Z. Wang, S.W. Remmenga, K.J. Rodabough, A.R. Karpf, J. Dong, J.S. Davis, C. Wang, G-1 Inhibits Breast Cancer Cell Growth via Targeting Colchicine-Binding Site of Tubulin to Interfere with

Chemical and Pharmaceutical Bulletin, **2020**, 68(12), 1184-1192.

Microtubule Assembly, Molecular cancer therapeutics, **2017**, 16(6), 1080-1091.

32. P. Barbier, A. Dorleans, F. Devred, L. Sanz, D. Allegro, C. Alfonso, M. Knossow, V. Peyrot, J.M. Andreu, Stathmin and Interfacial Microtubule Inhibitors Recognize a Naturally Curved Conformation of Tubulin Dimers, Journal of Biological Chemistry, **2010**, 285(41), 31672-31681.

33. S.Mirzaei, F.Eisvand, F.Hadizadeh, F.Mosaffa, A.Ghasemi, "Design, synthesis and biological evaluation of novel 5,6,7-trimethoxy-N-aryl-2-styrylquinolin-4-amines as potential anticancer agents and tubulin polymerization inhibitors", Bioorganic Chemistry, **2020**, 98:103711.

34. M. Afzal, J. Thathan, S. Jupudi, Pharmacophore modeling, atom-based 3D-QSAR, molecular docking and molecular dynamics studies on *Escherichia coli* ParE inhibitors, Computational Biology and Chemistry, **2020**, 84, 107197.

35. V. Yele, M.A. Azam, S. Jupudi, Ligand-based pharmacophore modeling, in silico virtual screening, molecular docking, and molecular dynamic simulation study to identify novel *Francisella tularensis* ParE inhibitors, Chemical papers, **2020**, 74, 4567-4580.

36. N.S. Tripuraneni, M.F. Azam, Pharmacophore modeling, 3D-QSAR and docking study of 2-phenyl pyrimidine analogs as selective PDE4B inhibitors, Journal of Theoretical Biology, **2016**, 394, 117-126.

37. S. Bhansali, V.M. Kulkarni, Pharmacophore generation, 3D-QSAR, docking study, virtual screening studies of p38-α mitogen-activated protein kinase inhibitors: pyridopyridazine-6-ones (part 2), 2013, **2014**, 4, 1-21.

38. http://gohom.win/ManualHom/Schrodinger_20152_docs/maestro/help_Maestro/phase/atom_based_qsar.html

39. P. Kirubakaran, K. Muthusamy, K.H. Singh, S. Nagamani, Ligand-based pharmacophore modeling; atom-based 3D-QSAR analysis and molecular docking studies of phosphoinositide-dependent kinase-1 inhibitors, Indian J. Pharmaceut. Sci., **2012**, 74, 141-51.

40. A. Golbraikh, A. Tropsha, Predictive QSAR modeling based on diversity sampling of experimental datasets for the training and test set selection, J. Comput. Aid. Mol. Des., **2002**, 16, 357-369.

41. Ligprep, version 2.5, Schrödinger, LLC, New York, **2012**.

42. Phase, version 4.4, Schrödinger, LLC, New York, **2012**.

43. S.L. Dixon, A.M. Smondyrev, E.H. Knoll, S.N. Rao, D.E. Shaw, R.A. Friesner, PHASE: a new engine for pharmacophore perception, 3D QSAR model development, and 3D database screening: 1. Methodology and preliminary results, J. Comput. Aided Mol. Des., **2006**, 20, 647-71.

44. S.J. Cottrell, V.J. Gillet, R. Taylor, D.J. Wilton, Generation of multiple pharmacophore hypotheses using multiobjective optimization techniques, Journal of computer-aided molecular design, **2004**, 18(11), 665-682.

45. S. Nagamani, C. Kesavan, K. Muthusamy, E-Pharmacophore mapping and docking studies on Vitamin D receptor (VDR), Bioinformation, **2012**, 8(5), 705-710.

46. Glide 6.7 User Manual, Schrodinger, LLC, May **2015**.

47. https://www.schrodinger.com/science-articles/docking-and-scoring

48. X.Y. Meng, H.X. Zhang, M. Mezei, M. Cui, Molecular Docking: A powerful approach for structure-based drug discovery, Curr Comput Aided Drug Des., **2012**, 7(2), 146-157.

49. S.D. Firke, A.M. Dhote, R.R. Patil, A.A. Shrikhedkar, S.J. Surana, Natural Antidiabetic Agents: Molecular Docking Study using the Extra Precision Method, Letters in Drug Design & Discovery, **2021**, 18(2), 143-171.

50. K. Prabhu, M.M. Mahto, V.K. Gopalakrishnan, Virtual Screening, Molecular Docking and Molecular Dynamics Studies for Discovery of Novel Vegfr-2 Inhibitors, International Journal of Pharmaceutical and Clinical Research, **2014**, 6(3), 221-229.

51. G.P. Mishra, D. Panigrahi, Molecular docking and ADMET study for searching multi-targeted antiviral compounds against SARS-CoV-2: A computational approach, International Journal of Applied Science and Engineering, **2020**, 18(2), 004.

52. QikProp 3.5 User Manual, Schrodinger, LLC, September **2012**.

53. S.M.Z. Hosen, M.S.H. Kabir, A. Hasanat, T.A. Chowdhury, N. Chakrabarty, S.K. Sarker, M.R. Habib, R. Dash, Docking and ADME/T analysis of silibinin as a potential inhibitor of EGFR kinase for ovarian cancer therapy, Journal of Applied Pharmaceutical Science, **2016**, 6(08), 001-005.